ISSN 2394-3777 (Print)
ISSN 2394-3785 (Online)
Available online at www.ijartet.com

International Journal of Advanced Research Trends in Engineering and Technology (IJARTET)
Vol. 2, Issue 9, September 2015

Design of Single-Stage Boost Inverter using Fuzzy Neural Network Control and Adaptive Control

PG SCHOLAR **DELEEPKUMAR.S**
ASSISTANT PROFESSOR **PRAKASH K M.E**
DEPARTMENT OF ELECTRICAL AND ELECTRONICS
SATYAM COLLEGE OF ENGINEERING AND TECHONOLOGY

***Abstract*–This study mainly focuses on the development of two newly-designed control strategies including an adaptive control scheme and a fuzzy-neural-network (FNN) control system for a single-stage boost inverter. First, the dynamic model of a single-stage boost inverter is analyzed and built for the later control manipulation. Then, a model-based adaptive control scheme and a model-free FNN control system with varied learning rates are designed sequentially. The effectiveness of the proposed adaptive control scheme and the proposed FNN control system is verified by experimental results of a 1kW single-stage boost inverter prototype, and their merits are indicated in comparison with a traditional double-loop proportional-integral (PI) control framework. Experimental results show that the superior FNN control system has significant improvements of 45.2% total harmonic distortion (THD) and 37.1% normalized-mean-square-error (NMSE) compared to the conventional double-loop PI control framework under nonlinear loads.**

Keywords **Adaptive control, Fuzzy neural network, Proportional-integral control, Voltage tracking control, Boost inverter.**

I. INTRODUCTION

Ever increasing energy consumption, soaring energy costs, and worsening global environmental conditions such as the greenhouse effect have all contributed to the increased interest in clean-energy generation systems, e.g., wind power [1]-[2], solar power [3]-[4], fuel cell [5]-[6], etc. For a lower dc-voltage clean-energy power conversion system [1]-[7], the existing technology for commercial applications mainly can be divided into the following two kinds. One is the transformer-based structure, which uses a dc-ac inverter to generate an ac utility line voltage by a step-up transformer. The other is the two-stage framework, which adopts a dc-dc boost converter to get a sufficient dc-bus voltage for the later dc-ac inverter to obtain an ac utility line voltage. However, the conversion efficiency of the transformer-based structure is very low due to the switching loss of the transformer. Moreover, the two-stage power conditioning system has inevitable drawbacks, such as being bulky, costly, and inefficient, because each stage has to have a high efficiency for a higher overall efficiency, and more than five active components are required [7]. For several practical concerns, it is desirable to generate an ac utility line voltage with larger amplitude than the input power source in a single stage. For renewable energy applications, the dc-ac inverter always operates at the stand-alone power-supply mode (e.g., small-size household appliance, electric vehicle, etc.) or the grid-connected power-supply mode (e.g., power plant). According to different operational modes, the closed-loop control method should control the output voltage with a pre-specified reference voltage and a low total harmonic distortion (THD) in the stand-alone power-supply mode, or manipulate the output current with a pre-specified reference current and a high power factor in the grid-connected power-supply mode. The scope of this study is related to the tracking of the reference voltage in the stand-alone power-supply mode. In addition, it focuses on various control design and experimental comparison for a single-stage boost inverter to overcome the drawbacks of a two-stage power conditioning system.

In the past researches, a single-stage boost inverter composed of two individual boost converters has received more attention due to its simple structure and easy understanding [8]. In this topology, both boost converters are driven by two 180 phase-shifted dc-biased sinusoidal references, and its differential output is an ac utility line voltage. The boost converter, also known as the step-up converter, is the basic dc-dc converter configuration with an output voltage higher than its input voltage. From the control point of view, the fundamental control frame for a boost converter is challenging because it is a bilinear system and also a non-minimum phase system with respect to the output to be controlled. The presence of unstable zero dynamics introduces a hard constraint on the achievable performance [9]-[10], and makes the control problem more complicated [11]-[13].

The control of a single-stage boost inverter is closely related to the voltage tracking control problem of the basic boost converter. Until now, its control problem is still a

ISSN 2394-3777 (Print)
ISSN 2394-3785 (Online)
Available online at www.ijartet.com

International Journal of Advanced Research Trends in Engineering and Technology (IJARTET)
Vol. 2, Issue 9, September 2015

major concern [8], [14]-[15]. Cáceres and Barbi [8] designed a sliding-mode control framework for a boost dc-ac inverter, and intended it to be used in uninterruptible power supply (UPS) and ac drive system. But, the control scheme in [8] seems to be impractical because strict sufficient conditions with the coefficients in the sliding surface should be satisfied. Cortes *et al.* [14] presented a numerical method to find an exact inductor current reference for handling the tracking control of a boost converter with a sinusoidal output voltage. However, detailed system dynamics were required in [14] such that the control performance was sensitive to system parameters. Sanchis *et al.* [15] proposed a double-loop regulation scheme with an inductor current control inner loop and an output voltage control outer loop for a single-stage boost inverter, which can be used in UPS, photovoltaic systems, etc. Although the requirement of detailed system dynamics has been relaxed in [15], the stability of the double-loop regulation scheme can not be completely guaranteed under the possible occurrence of operational conditions. In recent years, there are some applications to use single-stage boost inverters for the fuel cell system in standalone power supply [16] and in grid-connected power supply [17]. Jang and Agelidis [16] investigated a boost inverter to achieve boosting and inversion functions in a single stage for developing a fuel-cell-based energy system that offers high conversion efficiency, low cost, and compactness. Jang *et al.* [17] used the boost-inverter topology as a building block for a single-phase grid-connected fuel cell system offering low cost and compactness. Unfortunately, traditional proportional-integral (PI) control or proportional-resonant (PR) control frameworks were adopted in [16]-[17] such that the stability of these kinds of control systems could not be completely assured when system uncertainties exist, and [24]-[25]. The integrated FNN system possesses the merits of both fuzzy systems [22] (e.g., humanlike IF-THEN rules thinking and ease of incorporating expert knowledge) and neural networks [23] (e.g., learning and optimization abilities, and connectionist structures). By this way, one can bring the low-level learning and computational power of neural networks into fuzzy systems and also high-level, humanlike IF-THEN rule thinking and reasoning of fuzzy systems into neural networks.

Due to inherent instability and high non-linearity associated with the boost converter dynamics in the single-stage boost inverter, the control problem is usually quite challenging to power engineers, especially in model-free control design. In this study, three control strategies including PI control, adaptive control and FNN control are implemented for the voltage tracking control of a single-stage boost inverter, and the corresponding experimental results are provided to compare individual diversities.The control gains should be repeatedly tuned to ensure favorable performances. Furthermore, there are advanced boost-inverter investigations for multiple energy sources [18]-[19]. Garcia *et al.* [18] contributed a novel dual transformerless single-stage current source inverter fed by a proton exchange membrane fuel cell and a photovoltaic array. Danyali *et al.* [19] presented a new extendable single-stage multi-input dc-dc/ac boost converter for a battery-based energy system.

Conventional proportional-integral-derivative (PID)- type controllers are the most popular strategies in industry due to their simple control structure, ease of design and inexpensive cost [15], [20]. However, this model-free PID-type controller can not provide perfect control performance if the controlled plant is highly nonlinear and uncertain. In general, adaptive control is a popular strategy in coping with structured uncertainties and provides a good performance over a limited range [21]. But, detailed system parameters are always required in order to cancel nonlinear terms in the system dynamics. On the other hand, intelligent control techniques (fuzzy control or neural network control) have been adopted in the control field according to their powerful learning ability and unnecessary prior knowledge of the controlled plant in the design process [22]-[24]. Although the fuzzy logic technique allows the constructing of a control system based in a group of rules in a similar way as the human thought does, how to build appropriate rules is the major problem [22]. Neural network has an inherent ability to model complex processes, to compensate for unstructured uncertainties and even to control the system without a prior knowledge of system parameters. Unfortunately, the internal behavior is very ambiguous to understand, i.e., it lacks clarity in the nature of decision making [23]. Therefore, the concept of incorporating fuzzy logic into a neural network has grown into a popular research topic [12],

ISSN 2394-3777 (Print)
ISSN 2394-3785 (Online)
Available online at www.ijartet.com

International Journal of Advanced Research Trends in Engineering and Technology (IJARTET)
Vol. 2, Issue 9, September 2015

and have to be greater than V_{in} $0.5A_o$, in which A_o is the peak amplitude of the inverter output voltage. Moreover, the voltage gains of each boost converter can be obtained as

$$V_1 / V_{in} \quad 1/(1 \quad d_1) \tag{4}$$

$$V_2 / V_{in} \quad 1/(1 \quad d_2) \tag{5}$$

where d_1 and d_2 are the duty cycles for two boost converters, respectively.

To express the dynamic modeling, it is assumed that all the circuit components are ideal and the single-stage boost inverter is operated in a continuous conduction mode. Moreover, the circuit framework of the single-stage boost inverter in Fig. 1(a) can be equivalent to the one in Fig. 1(b). When the power switch S_2 is turned on, and the power switch S_1 is turned off, the input power source V_{in} charges the inductor L_1, and the capacitor C_1 releases its stored energy to the output terminal. On the contrary, when the power switch S_1 is turned on and the power switch S_2 is turned off, the energy stored in the inductor L_1 is released to the output terminal. The state-space average modeling [26] of the equivalent circuit in Fig. 1(b) with the state variables (i_{L1} and V_1) is given by

$$\dot{i}_{L1} \quad [V_{in} \quad (1 \quad d_1)V_1]/L_1 \tag{6}$$

$$\dot{V}_1 \quad \frac{1}{C_1}\left(\frac{V_1}{R_o} \quad \frac{V_2}{R_o}\right) \quad \frac{i_{L1}}{C_1}(1 \quad d_1) \tag{7}$$

where i_{L1} is the current passed through the inductor L_1. Similarly, the state-space average modeling with the state variables (i_{L2} and V_2) can be expressed as

$$\dot{i}_{L2} \quad [V_{in} \quad (1 \quad d_2)V_2]/L_2 \tag{8}$$

$$\dot{V}_2 \quad \frac{1}{C_2}\left(\frac{V_2}{R_o} \quad \frac{V_1}{R_o}\right) \quad \frac{i_{L2}}{C_2}(1 \quad d_2) \tag{9}$$

where i_{L2} is the current passed through the inductor L_2. By taking the converter output voltages (V_1 and V_2) as the system states under the occurrence of system uncertainties, (7) and (9) can be rearranged as

$$\begin{aligned} \dot{V}_1(t) \quad & a_{p1}V_1(t) \quad b_{p1}u_1(t) \quad c_{p1}(t) \quad d_{p1}(t) \\ & (a_{pn1} \quad a_{p1})V_1(t) \quad (b_{pn1} \quad b_{p1})u_1(t) \\ & (c_{pn1} \quad c_{p1}) \quad d_{p1}(t) \\ & a_{pn1}V_1(t) \quad b_{pn1}u_1(t) \quad c_{pn1}(t) \quad w_1(t) \end{aligned} \tag{10}$$

$$\begin{aligned} \dot{V}_2(t) \quad & a_{p2}V_2(t) \quad b_{p2}u_2(t) \quad c_{p2}(t) \quad d_{p2}(t) \\ & (a_{pn2} \quad a_{p2})V_2(t) \quad (b_{pn2} \quad b_{p2})u_2(t) \\ & (c_{pn2} \quad c_{p2}) \quad d_{p2}(t) \\ & a_{pn2}V_2(t) \quad b_{pn2}u_2(t) \quad c_{pn2}(t) \quad w_2(t) \end{aligned} \tag{11}$$

where $a_{p1} \quad 1/(R_oC_1)$; $a_{p2} \quad 1/(R_oC_2)$; $b_{p1} \quad k_1/C_1$; $b_{p2} \quad k_2/C_2$; $c_{p1} \quad i_{L1}/C_1 \quad V_2/(R_oC_1)$; $c_{p2} \quad i_{L2}/C_2 \quad V_1/(R_oC_2)$; $d_{p1} \quad (i_{L1} \quad k_1)u_1/C_1$; $d_{p2} \quad (i_{L2} \quad k_2)u_2/C_2$; $u_1 \quad d_1$ and $u_2 \quad d_2$ are control and c_{pn2} denote the nominal values of a_{p1}, a_{p2}, b_{p1}, b_{p2}, c_{p1} and c_{p2}, respectively; a_{p1}, a_{p2}, b_{p1}, b_{p2}, c_{p1} and c_{p2} represent the system parameter variations; k_1 and k_2 are extra designed positive coefficients to avoid the inverse of control gains dividing by the currents (i_{L1} and i_{L2}); $w_1(t)$ and $w_2(t)$ are the lumped uncertainties and defined as

$$w_1(t) \quad a_{p1}V_1 \quad b_{p1}u_1 \quad c_{p1} \quad d_{p1} \tag{12}$$

$$w_2(t) \quad a_{p2}V_2 \quad b_{p2}u_2 \quad c_{p2} \quad d_{p2} \tag{13}$$

Here, the bounds of the lumped uncertainties are assumed to be given; that are

$$|w_1(t)| \quad _1 \text{ and } |w_2(t)| \quad _2 \tag{14}$$

where $|\ |$ is the operator of an absolute value; $_1$ and $_2$ are given positive constants. From (10) and (11), the inverter output voltage can be expressed as

$$\begin{aligned} V_o(t) \quad & V_1(t) \quad V_2(t) \quad a_{pn1}V_1(t) \quad b_{pn1}u_1(t) \quad c_{pn1}(t) \\ & w_1(t) \quad a_{pn2}V_2(t) \quad b_{pn2}u_2(t) \quad c_{pn2}(t) \quad w_2(t) \end{aligned} \tag{15}$$

The control problem is to design suitable control efforts (u_1 and u_2) to force the system states (V_1 and V_2 to track reference converter output voltages (V_{1ref} and V_{2ref}) under the possible occurrence of system uncertainties. In other words, the inverter output voltage (V_o) also can track its reference sinusoidal command (V_{oref}) if the voltage tracking errors of two boost converters can converge to zero.

III. Control System Design

A. Double-Loop PI Control

In industrial applications, the double-loop proportional-integral (PI)-type control is usually used due to its simple scheme, ease of design, and inexpensive cost [20]. A double-loop PI control system [15] is adopted in this study. Define the voltage tracking errors of two boost converters in the outer loop as

$$e_{v1} \quad V_{1ref} \quad V_1 \tag{16}$$

$$e_{v2} \quad V_{2ref} \quad V_2 \tag{17}$$

where V_{1ref} and V_{2ref} are the refernce converter output voltages. The reference inductor currents i_{L1ref} and i_{L2ref} are generated through PI voltage controllers according to the converter voltage tracking errors (e_{v1} and e_{v2}). Moreover, the current tracking errors of two boost converters in the inner loop are defined as

$$e_{i1} \quad i_{L1ref} \quad i_{L1} \tag{18}$$

$$e_{i2} \quad i_{L2ref} \quad i_{L2} \tag{19}$$

ISSN 2394-3777 (Print)
ISSN 2394-3785 (Online)
Available online at www.ijartet.com

International Journal of Advanced Research Trends in Engineering and Technology (IJARTET)
Vol. 2, Issue 9, September 2015

tracking errors (e_{i1} and e_{i2}). In this study, the PI control formula can be generally represented as

$$u \quad u_P \quad u_I \quad k_P e \quad k_I \int_0^t e \, d \tag{20}$$

where u_P is a proportional controller; u_I is an integral controller; k_P and k_I are the corresponding control gains. Selection of the values for the gains in the PI control system has a significant effect on the control performance [20]. In general, they are determined according to desirable system responses, e.g., rising time, settling time, etc. The major drawbacks of a traditional PI control framework are recited as follows. (i) The PI gains usually need manual retuning before being transferred to the process under different operational conditions. (ii) The PI-type controller can not provide favorable control performance if the controlled plant has nonlinear and uncertain factors (e.g., the occurrence of a nonlinear load).

B. Adaptive Control

In order to control the single-stage boost inverter more effectively, a new adaptive control system is proposed. The objective of the proposed adaptive control for the single-stage boost inverter is to force the system state (V_o) to track a reference inverter output voltage (V_{oref}) under the possible occurrence of system uncertainties. Define an inverter voltage tracking error (e_{vo}) as

$$e_{vo} \quad V_{oref} \quad V_o \quad V_{1ref} \quad V_1 \quad V_{2ref} \quad V_2 \tag{21}$$

According to (15) and (21), the derivative of the inverter voltage tracking error can be expressed as

$$\begin{aligned} e_{vo} \quad & V_{1ref} \quad a_{pn1} V_1(t) \quad b_{pn1} u_1(t) \quad c_{pn1}(t) \quad w_1(t) \\ & V_{2ref} \quad a_{pn2} V_2(t) \quad b_{pn2} u_2(t) \quad c_{pn2}(t) \quad w_2(t) \end{aligned} \tag{22}$$

Consider a Lyapunov function candidate as

$$V_L \quad e_{vo}^2 \quad / \; 2 \tag{23}$$

By taking the derivative of V_L with respect to time, one can obtain

$$\begin{aligned} V_L \quad & e_{vo} e_{vo} \quad e_{vo} [V_{1ref} \quad a_{pn1} V_1(t) \quad b_{pn1} u_1(t) \quad c_{pn1}(t) \\ & w_1(t) \quad V_{2ref} \quad a_{pn2} V_2(t) \quad b_{pn2} u_2(t) \quad c_{pn2}(t) \quad w_2(t)] \end{aligned} \tag{24}$$

By observing (24), one should design two control efforts (u_1 and u_2) to respectively deal with the system dynamic and uncertainty terms ($V_{1ref} a_{pn1} V_1(t)$ $c_{pn1}(t)$ $w_1(t)$ and $w_2(t)$) for making the derivative of V_L to be a negative-definite function. Thus, the proposed adaptive control laws for the single-stage boost inverter can be designed as

$$\begin{aligned} u_1 \quad & b_{pn1}^{-1} [\; a_{pn1} V_1 \quad V_{1ref} \quad c_{pn1} \quad {}_1 \operatorname{sgn}(e_{vo}) \\ & k_{p1} e_{vo} \quad k_i \int_0^t e_{v1} d \;] \end{aligned} \tag{25}$$

$$\begin{aligned} u_2 \quad & b_{pn2}^{-1} [\; a_{pn2} V_2 \quad V_{2ref} \quad c_{pn2} \quad {}_2 \operatorname{sgn}(e_{vo}) \\ & k e \end{aligned} \tag{26}$$

where k_{p1}, k_{p2} and k_i are positive gains; sgn( ) is a sign function. By substituting (25)-(26) into (24), one can obtain

$$\begin{aligned} V_L \quad & k_{p1} e_{vo}^2 \quad k_{p2} e_{vo}^2 \quad k_i \int_0^t e_{vo}^2 \, d \quad |e_{vo}| \; [\quad |w_1| \;] \\ & |e_{vo}| \; [\; {}_2 \quad |w_2| \;] \quad k_{p1} e_{vo}^2 \quad k_{p2} e_{vo}^2 \quad 0 \end{aligned} \tag{27}$$

As can be seen from (27), it can imply that the inverter voltage tracking error e_{vo} go to zero asymptotically because the derivative of V_L is a negative-definite function. According to Lyapunov theorem [21], the stability of the adaptive control scheme for the single-stage boost inverter can be guaranteed if the condition of ${}_1$ $|w_1(t)|$ and ${}_2$ $|w_2(t)|$ can be satisfied.

C. FNN Control System

A fuzzy neural network (FNN) control system with a four-layer network structure composed of the input (i layer), membership (j layer), rule (k layer) and output (o layer) layers is adopted [12]. The membership layer acts as the membership functions. Moreover, all the nodes in the rule layer form a fuzzy rule base. The signal propagation and the basic function in each layer of the FNN are introduced as follows.

For every node i in the input layer transmits the input variables x_i ($i \quad 1, \square, n$) to the next layer directly, and n is the total number of the input nodes. Moreover, each node in the membership layer performs a membership function. In this study, the membership layer represents the input values with the following Gaussian membership functions:

$$net_j(x_i) \quad \frac{(x \quad m_i^j)^2}{(\quad {}_i^j)^2}, \quad {}_i^j(net_j(x_i)) \exp(net_j(x_i)) \tag{28}$$

where exp(.) is the exponential operator; m_i^j and ${}_i^j$ ($i \quad 1, \square, n; j \quad 1, \square, n_{pi}$) , respectively, are the mean and the standard deviation of the Gaussian function in the j-th term of the i-th input variable x_i to the node of this layer. In order to represent the general case including different clusters with respect to the network inputs, the symbol n_{p_i} is utilized to denote the individual number of the linguistic and variable with respect to each input node. $n_r \sum_{i \; 1} n_p \; V_{2ref} \quad a_{pn2} V_2(t) \quad c_{pn2}(t)$ represents the total number of membership functions. In addition, each node k in the rule layer is denoted by , which multiplies the input signals and outputs the result of the product. The output of this layer is given as

$$k \quad \prod_{i \; 1}^{n} w_{ji}^k \; {}_i^j(net_j(x_i)) \tag{29}$$

where $_k$ ($k \; 1, \square, n_y$) represents the k-th output of the rule layer; w_{ji}^k are the weights between the membership layer and the rule layer and are assumed to be unity; n_y is

ISSN 2394-3777 (Print)
ISSN 2394-3785 (Online)
Available online at www.ijartet.com

International Journal of Advanced Research Trends in Engineering and Technology (IJARTET)
Vol. 2, Issue 9, September 2015

of (29) represents the product operation of the membership grade from the membership layer in the j-th term of the i-th input variable. The range of j is from 1 to n_{pi}. By considering full rule combinations, the number of rules can be represented as $n_y = \prod_{i=1}^{n} n_{pi}$. This product operation is utilized to determine the firing strength. It can be referred as the fuzzy inference mechanism. Furthermore, the output node together with links connected it act as a defuzzification procedure. Each node y_o ($o = 1, \ldots, n_o$) computes the overall output as the summation of all input signals with the following type:

$$y^o = f_o^o\left(\sum_{k=1}^{n_y} (w^o)_k^k f^o(\cdot)\right) \quad / [1 + \exp(-)] \tag{30}$$

where $f_o(\cdot)$ is the sigmoid activation function; $\sum_{k=1}^{n_y} w_k$; is a positive constant; w_k is the output action strength of the o-th output associated with the k-th rule. In this study, the inputs of the FNN control system are the voltage tracking errors ($x_1 = e_{v1}$ and $x_2 = e_{v2}$), and its outputs are the control efforts ($y_1 = u_1$ and $y_2 = u_2$) for the single-stage boost inverter. In general, the outputs of the conventional control law can not be guaranteed to be inside the range (0~1) for the duty cycles of the power switches in the boost inverter, so that the corresponding control parameters should be carefully selected to avoid the occurrence of the PWM saturation. As can be seen from the design of the FNN output in (30), the utilization of the sigmoid activation function can be directly supplied to the duty cycles of the power switches in the boost inverter without strict constraints on control parameters selection.

To describe the on-line learning algorithm of this FNN control system via supervised gradient descent method, first the energy function E is defined as

$$E = (e_{vo}^2 + e_{v1}^2 + e_{v2}^2)/2 \tag{31}$$

In the output layer, the error terms to be propagated are given as

$$\frac{E}{y_1} = (e_{vo} + e_{v1})V_{in} \tag{32a}$$

$$\frac{E}{y_2} = (e_{v2} + e_{vo})V_{in} \tag{32b}$$

where and are positive gains to be designed by the user. In this study, the design of and is helpful to avoid the terms in (32) dividing by zero, where and are positive

$$w_k^o(N+1) = w_k^o(N) + \Delta w_k^o \tag{34}$$

where N denotes the number of iterations. Since the weights in the rule layer are unified, only the error term should be calculated and propagated.

$$\frac{E}{} = w_1^1 f_1 + w_2^2 f_2 \tag{35}$$

In the membership layer, the error term is computed as follows:

$$\frac{E}{net_j(x_i)} = \sum_{k=1}^{n_y} \tag{36}$$

The update laws of and can be obtained as

$$m_i(N+1) = m_i(N) + \Delta m_i \text{ with}$$

$$\frac{E}{m_i} \quad 2(x - m^j) \tag{37}$$

$$(N+1) = (N) + \Delta \text{ with}$$

$$\frac{E}{} \quad \frac{2(x_i - m^j)^2}{(\quad)} \tag{38}$$

where and are the learning-rate parameters of the mean and the standard deviation of the Gaussian function. Selection of the values for the learning-rate parameters has a significant effect on the network performance. In order to train the FNN effectively, varied learning rates, which guarantee convergence of the voltage tracking errors based on the analyses of a discrete-type Lyapunov function, are adopted [25]. Consider the energy function in (31) as a discrete-type Lyapunov function, and the change in the Lyapunov function can be written as

$$E(N) = E(N+1) - E(N) \tag{39}$$

Then, the linearized model of the energy function [25] can be approximately represented by

$$E(N+1) - E(N) = \Delta E(N) \approx \sum_{o=1}^{n_o}\sum_{k=1}^{n_y}\left[\frac{E(N)}{w_k^o}\Delta w_k^o\right] + \sum_{i=1}^{n}\sum_{j=1}^{n_j}\left[\frac{E(N)}{m_i^j}\Delta m_i^j + \frac{E(N)}{\sigma_i^j}\Delta \sigma_i^j\right] \tag{40}$$

According to (33), (37) and (38), (40) can be rewritten as

$$E(N+1) - E(N) = -\frac{1}{3}\left|\frac{w}{E(N)}\sum_{o=1}^{n_o}\sum_{k=1}^{n_y}\left(\frac{E(N)\,y_o}{y_o\,w_k^o}\right)\right|$$

$$-E(N)\left|\frac{1}{3}\frac{m}{E(N)}\sum_{i=1}^{n}\sum_{j=1}^{n_{pi}}\sum_{o=1}^{n_o}\sum_{k=1}^{n_y}\left|\frac{E(N)\,y_o}{y_o\,u_i^j}\right|^2\left|\frac{y_o}{m_i^j}\right|^2\right|$$

$$E(N)\left|\frac{1}{3}\frac{}{E(N)}\sum_{i=1}^{n}\sum_{j=1}^{n_{pi}}\sum_{o=1}^{n_o}\sum_{k=1}^{n_y}\left|\frac{E(N)\,y_o}{y_o\,u_i^j}\right|^2\left|\frac{y_o}{\sigma_i^j}\right|^2\right|$$

ISSN 2394-3777 (Print)
ISSN 2394-3785 (Online)
Available online at www.ijartet.com

International Journal of Advanced Research Trends in Engineering and Technology (IJARTET)
Vol. 2, Issue 9, September 2015

in the output layer, the change of the mean and standard deviation in the Gaussian function, respectively; $|\ |$ is the absolute value operator; b_w $\sum_{o=1}^{n_y}\sum_{k=1}^{n_o}\left(\frac{E(N)\ y_o}{y_o\ \ o\ \ k\ \ w_k^o}\right)$; b_m $\sum_{i=1}^{n_{pi}}\sum_{j=1}^{n_o}\sum_{o=1}^{n_y}\sum_{k=1}^{n_o}\left(\frac{E(N)\ y_o\ \ o\ \ k\ \ i^j}{y_o\ \ o\ \ k\ \ u_i^j\ \ m_i^j}\right)$; b_s $\sum_{i=1}^{n}\sum_{j=1}^{n_{pi}}\sum_{o=1}^{n_o}\sum_{k=1}^{n_y}\left(\frac{E(N)\ y_o\ \ o\ \ k\ \ i^j}{y_o\ \ o\ \ k\ \ u_i^j\ \ i^j}\right)$. If the learning-rate parameters of the FNN are designed as

$$w \quad \frac{E(N)}{3(b_w^2)}, \quad m \quad \frac{E(N)}{3(b_m^2)}, \quad s \quad \frac{E(N)}{3(b_s^2)} \qquad (42)$$

where is a small positive constant. The total amount of $\left|\frac{1}{3}\ \ \frac{w}{E(N)}b_w^2\right|$, $\left|\frac{m}{E(N)}b_m^2\right|$, and $\left|\frac{1}{3}\ \ \frac{s}{E(N)}b_s^2\right|$ is less than one, i.e., $E(N+1) < E(N)$. Thus, the Lyapunov stability of $E(N) \to 0$ and $E(N) = 0$ can be guaranteed according to (39) [21]. Moreover, the voltage tracking errors will converge to zero gradually.

The superior learning of FNN with varied learning rates can be found in published literatures [24], [25]. Since the best values of the learning rates at the beginning of learning may be not as good in later learning, a more efficient approach in [24] is used to update the learning rates according to the decreasing or increasing of the energy function E. However, the system stability can not be guaranteed by the approach in [24]. Wai and Liu [25] investigated varied learning rates for a dynamic Petri recurrent-fuzzy-neural-network, and this network structure was applied to the path tracking control of a mobile robot. Although the convergence of path tracking errors can be guaranteed in [25], it will cause the chattering phenomena during the learning process because the system sensitivity in [25] is approximated by the sign function. The major contributions of the proposed FNN control system are recited as follows. (i) The utilization of the sigmoid activation function in the FNN output (30) to be directly supplied for the duty cycles of the power switches in the boost inverter without strict constraints on control parameters selection. (ii) The derivation of varied learning rates in (42) to guarantee the convergence of the voltage tracking errors without the approximation of system sensitivity. Wai and Shih [12] designed an adaptive fuzzy-neural-network control (AFNNC) scheme for the voltage tracking control of a conventional dc-dc boost converter. However, system dynamic parameters were used for the adaptation laws of the network parameters. The difference between the major techniques in [12] and this study is the proposed FNN control system without the detailed system information.

output voltage of a single-stage boost inverter are set at V_{in} 48V and V_{oref} $110\sqrt{2}\sin(377t)$, respectively. Moreover, the prototype of the boost inverter is designed with the maximum output power, $P_{o(\max)}$ 1kW. In this boost inverter, two IGBT modules including four power switches are adopted, and the corresponding circuit components are selected as L_1 L_2 200 H and C_1 C_2 30 F.

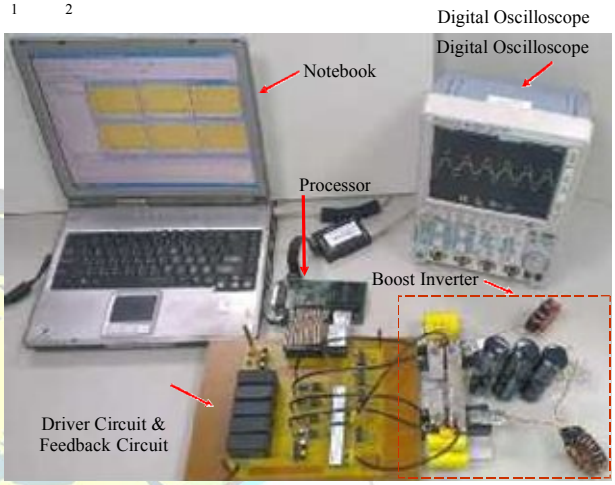

Fig. 2. Practical photograph of experimental equipment.

Figure 2 shows the practical photograph of the entire experimental setup. In the experiments, all the control methodologies are carried out using a digital-signal processor (DSP) TMS320F2812 with 150μ s sample time, manufactured by Texas Instruments. The TMS320F2812 chip has a system cycle of 6.67ns, a 32bit fixed point central arithmetic logic unit, 32bit accumulators, multipliers, and registers. Isolation amplifiers (AD202JN) and operational amplifiers (LM741) are used in the voltage feedback circuit to obtain the output voltages of two boost converters and the single-stage boost inverter for the utilization of the double-loop proportional-integral (PI) control framework, the adaptive control scheme, and the fuzzy neural network (FNN) control system. The measured ac output voltage is firstly fed into the AD202JN through the resistive voltage divider, and then the AD202JN produces a varied dc signal. Moreover, the operational amplifiers are used to adjust the DC offset and gain of this feedback signal to an appropriate value before feeding into the analog/digital converter (ADC) of the DSP board. Hall sensors (LA100) and operational amplifiers (LM741) are used in the current feedback circuit to sense the inductor currents. When the measured current flows through the winding on the LA100, a signal is produced by a magnetic coupling circuit inside the LA100. In addition, the operational amplifiers are used to adjust the dc offset and gain of the feedback signal to an appropriate value before feeding into the ADC of the DSP board.

ISSN 2394-3777 (Print)
ISSN 2394-3785 (Online)
Available online at www.ijartet.com

International Journal of Advanced Research Trends in Engineering and Technology (IJARTET)
Vol. 2, Issue 9, September 2015

circuits to execute the double-loop PI control framework, the adaptive control scheme, and the FNN control system, respectively.

The control parameters in the double-loop PI control framework, the adaptive control scheme, and the FNN control system are given as follows:

$$k_{Pv1} \quad k_{Pv\ 2}\ 0.08\ , \quad k_{Iv1}\ k_{Iv\ 2}\ 800 \quad k_{Pi1}\ k_{Pi\ 2}\ 0.05$$
$$k_{Ii1} \quad k_{Ii\ 2}\ 18.05\ , \quad k_1\ k_2 \quad 24\ , \quad k_{p1}\ k_{p\ 2}\ 65\ ,$$
$$k_i \quad 2800 \quad , \ _1 \quad _2 \quad 0.86 \quad , \ _1 \quad _2 \quad 0.054 \quad ,$$
$$0.01\ , \quad 0.83 \qquad (43)$$

where k_{Pv1}, $k_{Pv\,2}$, k_{Iv1} and $k_{Iv\,2}$ are the proportional and integral gains in the outer loop of the PI voltage controller; k_{Pi1}, $k_{Pi\,2}$, k_{Ii1} and $k_{Ii\,2}$ are the proportional and integral gains in the inner loop of the PI current controller. As for the double-loop PI control design, the bandwidth is designed as 3kHz for the inner current control loop and 300Hz for the outer voltage control loop. 50º-phase margins are specified for both loops. With these specifications, the proportional and integral constants of the PI current controller are 0.05 and 18.05, respectively, while they are 0.08 and 800, respectively, for the PI voltage controller. In (43), the values of k_1 k_2 24 are selected to avoid the inverse of control gains dividing by the currents (i_{L1} and i_{L2}). When small values of $_1$ $_2$ 0.86 are selected to alleviate the chattering phenomenon, the larger values of k_{p1} $k_{p\,2}$ 65 and k_i 2800 are set to cope with the possible occurrence of the worst cases $_1$ $|w_1(t)|$ and $_2$ $|w_2(t)|$. The selection of $_1$ $_2$ 0.054 is helpful to avoid the error terms in the output layer of the FNN dividing by zero; a small value of 0.01 is selected to avoid varied learning rates dividing by zero. The value of 0.83 is selected to curb the output of the FNN to be inside the reasonable range for the duty cycle of the power switch in the boost inverter. In this study, the inputs of the FNN are the voltage tracking errors (e_{v1} and $e_{v\ 2}$); i.e., n=2. Moreover, the outputs of the FNN are the control efforts (u_1 and u_2); i.e., n_o 2 . In order to achieve the lowest computation burden in practice, the associated fuzzy sets with Gaussian function for each input signal are equally divided into N (negative), Z (zero), and P (positive); i.e., n_{p_1} 3 and n_{p_2} 3 (n_r 3 3 6). One can obtain the

(b)

and e_{v2} . The effect due to the inaccurate selection of the initialized parameters can be retrieved by the on-line learning methodology.

The following normalized-mean-square-error (NMSE) value of the voltage tracking response is used for examining the control performance:

$$NMSE(x) \quad \frac{1}{x_{\max} T} \sum_{n\ 1}^{T} x^2 \quad (n) \qquad (44)$$

where x is the inverter voltage tracking error (e_{vo}); $x_{\max}$ is the amplitude of the voltage command; T is the total sampling instant. As can be seen from the lumped uncertainties in (12) and (13), the change of load will influence the system parameters (a_{p1}, a_{p2}, c_{p1} and $c_{p\,2}$). Thus, the output power varied between 500W and 1kW, the condition of a nonlinear load, and the input voltage varied with 48V±15% will be used to examine the transient behavior and the ability of the control strategies to tolerate the system (parameters) uncertainties in the experiments.

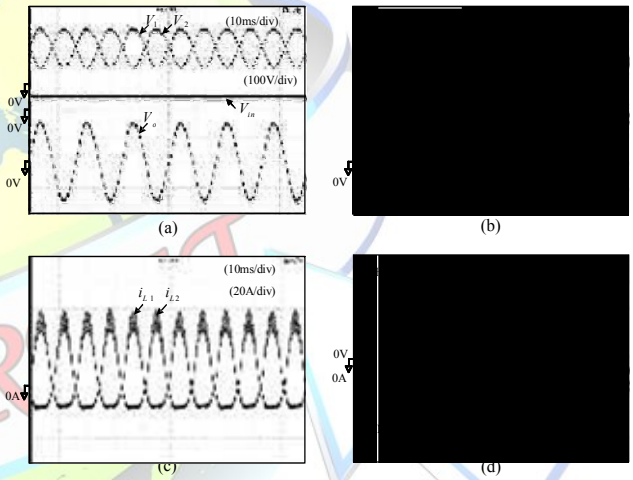

Fig. 3. Experimental results of PI control at 1kW output power.

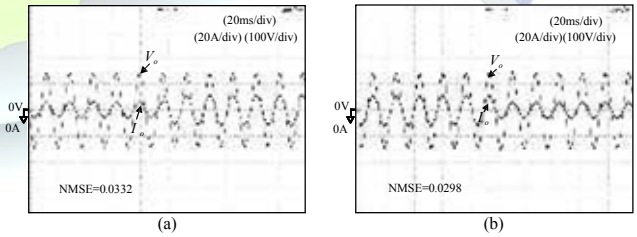

Fig. 4. Experimental results of PI control under output power variations: (a) Output power changes from 500W to 1kW; (b) Output power changes from 1kW to 500W.

ISSN 2394-3777 (Print)
ISSN 2394-3785 (Online)
Available online at www.ijartet.com

International Journal of Advanced Research Trends in Engineering and Technology (IJARTET)
Vol. 2, Issue 9, September 2015

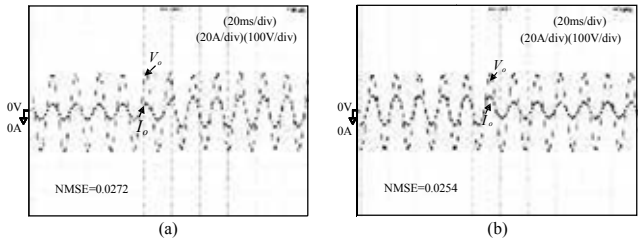

Fig. 6. Experimental results of adaptive control under output power variations: (a) Output power changes from 500W to 1kW; (b) Output power changes from 1kW to 500W.

The experimental results of the proposed adaptive control scheme for the boost inverter at 1kW output power are depicted in Fig. 5. To compare Fig. 3 with Fig. 5, the proposed adaptive control scheme provides better voltage tracking responses with lower THD and NMSE values. Moreover, the experimental results of the proposed adaptive control system for the boost inverter under output power variations are depicted in Fig. 6, where the output power changes from 500W to 1kW in subfigure (a), and the output power changes from 1kW to 500W in subfigure (b). It is obvious that the NMSE values (0.0332 and 0.0298) under the occurrence of load variations in Fig. 4 are reduced to (0.0272 and 0.0254) by the proposed adaptive control scheme. By observing Fig. 6, the transient time of the proposed adaptive control scheme for the boost inverter under load variations is less than 2ms.

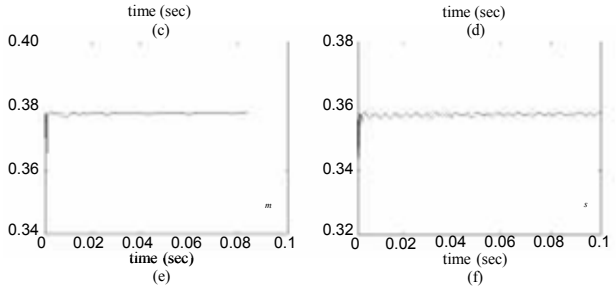

Fig. 8. Experimental network parameters of FNN control system: (a) $\|\boldsymbol{m}\|$; (b)$\|\ \|$; (c) $\|\boldsymbol{w}\|$; (d) $_{w}$; (e) $_{m}$; (f) $_{s}$.

The experimental results of the proposed FNN control system for the boost inverter at 1kW output power are depicted in Fig. 7. In comparison with the adopted PI control framework and the proposed adaptive control scheme, the proposed FNN control system yields superior voltage tracking responses with lower THD and NMSE values. For ease of notation, define adjustable parameter vectors $\boldsymbol{m}$, and $\boldsymbol{w}$ collecting all the means and standard deviations of the Gaussian functions and the weights in the output layer as $\boldsymbol{m}$ $[m^1_1 \square m^{n_{p1}}_1\ m^1_2 \square m^{n_{p2}}_2 \square m^1_n \square m^{n_{pn}}_n]_n$, $\boldsymbol{\sigma}$ $[\ _1^1 \square\ _1^{n_{p1}}\ _2^1 \square\ _2^{n_{p2}} \square\ _n^1 \square\ _n^{n_{pn}}]$, and $\boldsymbol{w}$ $[w^1_1 \square w^1_{n_y}$

ISSN 2394-3777 (Print)
ISSN 2394-3785 (Online)
Available online at www.ijartet.com

International Journal of Advanced Research Trends in Engineering and Technology (IJARTET)
Vol. 2, Issue 9, September 2015

$w_1^2 \square w_{n_y}^2 \square w_1^{n_o} \square w_{n_y}^{n_o}]$. These free parameter changes during the voltage tracking of the boost inverter can be observed from Fig. 8(a)-(c), in which $\| \|$ denotes the Euclidean norm. Moreover, the adaptations of the learning rates as the boost inverter tracks its desired output voltage are also depicted in Fig. 8(d)-(f). It is evident that the learning rates changes during the trasient process to handle the real environment, and all the tuned parameters can be constricted to ensure the stabilityof the internal states.

The experimental results of the proposed FNN control system for the boost inverter under output power variations are depicted in Fig. 9, where the output power changes from 500W to 1kW in subfigure (a), and the output power changes from 1kW to 500W in subfigure (b). It is obvious that the NMSE values (0.0332 and 0.0298) under the occurrence of load variations in Fig. 4 are reduced to (0.0231 and 0.0211) by the proposed FNN control system with varied learning rates. As can be seen from Fig. 9, there is no output current oscillation during the output power variations between 500W and 1kW by the proposed FNN control system. By observing Fig. 9, the transient time of the proposed FNN control system for the boost inverter under load variations is less than 1ms.

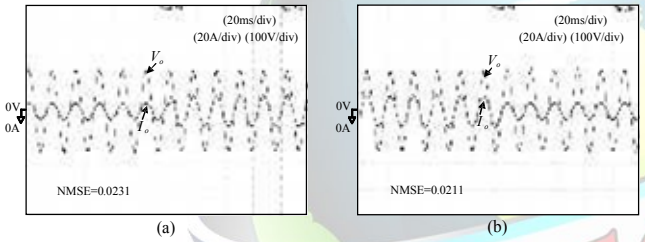

Fig. 9. Experimental results of FNN control under output power variations: (a) Output power changes from 500W to 1kW; (b) Output power changes from 1kW to 500W.

The experimental results of the single-stage boost inverter under nonlinear loads (i.e., resistor (300Ω)-inductor (500μ H)-capacitor (180μ F) RLC load) are depicted in Fig. 10, where the subfigure (a) is the response of the adopted PI control framework, the subfigure (b) is the response of the proposed adaptive control scheme, the subfigure (c) is the response of the proposed FNN control system, and the subfigure (d) is the running time for per cycle in individual control strategies. As can be seen from Fig. 10, the THD and NMSE values (5.24% and 0.0448) induced by the adopted PI control framework can be reduced to be 3.32% and 0.0335 by the proposed adaptive control scheme, and to be 2.87% and 0.0282 by the proposed FNN control system with varied learning rates. The THD values of the proposed adaptive control scheme and the proposed FNN control system can be properly controlled less than 5% to comply with the international standard compliance (e.g., the IEEE standard 1547-2003). The experimental records for the THD and NMSE values of the adopted PI control framework, the proposed adaptive control scheme, and the proposed FNN control system for the single-stage boost inverter at examined conditions are summarized in Table I. As can be seen from Fig. 10(d), the running times for per cycle in the double-loop PI control framework, the adaptive control scheme, and the FNN control system are 34.5μ s, 40.5μ s, and 117μ s, respectively. Although the computational costs of the proposed adaptive control scheme and the proposed FNN control system are higher than the one of the double-loop PI control framework, the proposed adaptive control scheme has over 8% THD and 14.8% NMSE improvements than the double-loop PI control framework; the proposed FNN control system with varied learning rates has over 14.4% THD and 29.3% NMSE improvements than the double-loop PI control framework. Due to the increasingly requirement of various functions in the power conditioners, microchips or micro-controllers are always taken as the control center in recent years. Because the operation speed of microchips or micro-controllers is substantially increased in the past decade, and the control interval is set at 150μ s in this study, the interval time is long enough to execute the proposed adaptive control scheme and the proposed FNN control system in practical applications. According to experimental results in Figs. 3-10, the proposed FNN control system indeed yields superior transient and steady-state voltage tracking control performance than the adopted PI control framework and the proposed adaptive control scheme under the possible occurrence of system uncertainties.

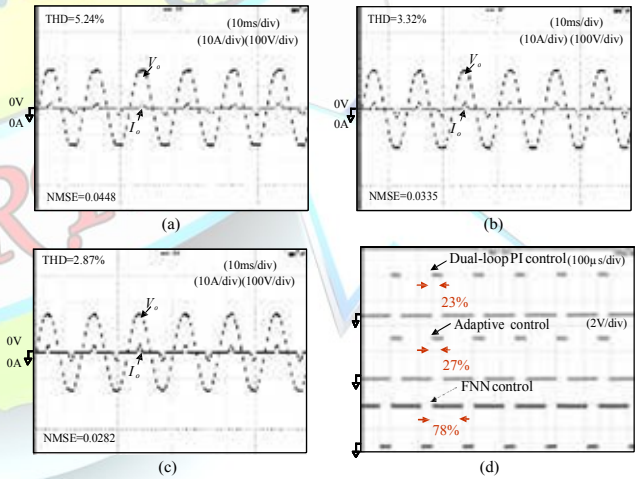

ISSN 2394-3777 (Print)
ISSN 2394-3785 (Online)
Available online at www.ijartet.com

International Journal of Advanced Research Trends in Engineering and Technology (IJARTET)
Vol. 2, Issue 9, September 2015

Fig. 10. Experimental results under nonlinear loads: (a) PI control; (b) Adaptive control; (c) FNN control; (d) Running time for per cycle in individual control strategies.

Table I.

EXPERIMENTAL PERFORMANCE COMPARISONS OF PI CONTROL, ADAPTIVE CONTROL AND FNN CONTROL FOR SINGLE-STAGE BOOST INVERTER

Control / Test condition	PI control		Adaptive control		FNN control	
	THD	NMSE	THD	NMSE	THD	NMSE
Output power 1kW	3.12%	0.0276	2.87%	0.0220	2.67%	0.0195
Output power variation from 500W to 1kW		0.0332		0.0272		0.0231
Output power variation from 1kW to 500W		0.0298		0.0254		0.0211
Nonlinear load	5.24%	0.0448	3.32%	0.0335	2.87%	0.0282

ISSN 2394-3777 (Print)
ISSN 2394-3785 (Online)
Available online at www.ijartet.com

International Journal of Advanced Research Trends in Engineering and Technology (IJARTET)
Vol. 2, Issue 9, September 2015

In order to imitate renewable energy applications with the input dc voltage variations (e.g., photovoltaic voltage varied with solar irradiation), Figure 11 exhibits the experimental output voltage regulation characteristics of the proposed FNN control system against the change of the input voltage, where the response of the input voltage variation from 48V to 40.8V (-15%) with 500W output power is depicted in Fig. 11(a); the response of the input voltage variation from 48V to 55.2V (+15%) with 500W output power is depicted in Fig. 11(b). As can be seen from this figure, the proposed FNN control system, which is less sensitive to the input voltage variation, also can get favorable transient and steady-state voltage control performance under varied input voltages.

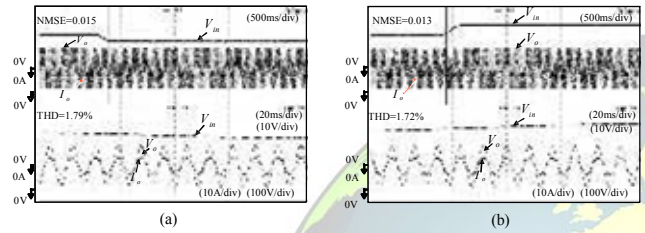

Fig. 11. Experimental results of FNN control under input voltage variations: (a) Input voltage changes from 48V to 40.8V; (b) Input voltage changes from 48V to 55.2V.

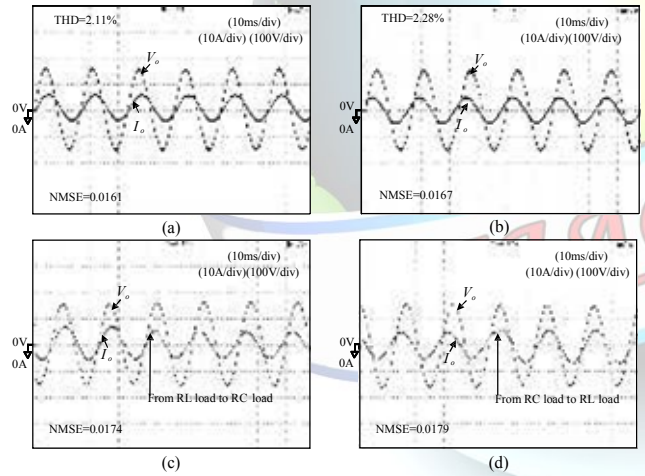

Fig. 12. Experimental results of boost inverter with FNN control for various loads with different power factors: (a) RL load; (b) RC load; (c) Varied from RL load to RC load; (c) Varied from RC load to RL load.

For testing the ability of the boost inverter with the superior FNN control system for various loads with different power factors, the resistor-inductor (RL) load with a power factor of 0.9 lagging and the resistor-capacitor (RC) load with a power factor of 0.82 leading are adopted. The experimental results at various loads are depicted in Fig. 12. The inverter output voltage and current under the RL load is depicted in Fig. 12(a), where the THD and NMSE records are 2.11% and 0.0161, respectively. The inverter output voltage and current under the RC load is depicted in Fig. 12(b), where the THD and NMSE records are 2.28% and 0.0167, respectively. Figure 12(c) shows the inverter output voltage and current under the variation from the RL load to the RC load; the ones under the variation from the RC load to the RL load is depicted in Fig. 12(d). The NMSE records in Fig. 12(c) and (d) are 0.0174 and 0.0179, respectively. As can be seen from Fig. 12, the proposed FNN control system can provide favorable control performance under the changes of load power factors.

In order to examine the effectiveness of the boost inverter with the superior FNN control system for real household appliances, a fourteen-inch electric fan with a rated voltage $110V_{rms}$ and a rated power 100W (power factor =0.98 lagging) is adopted here. The experimental output voltage and current at the middle wind velocity is depicted in Fig. 13(a), where the THD and NMSE records are 0.54% and 0.0021, respectively. Moreover, the experimental result under the wind velocity changed from the middle level to the large level is depicted in Fig. 13(b), and the one under the wind velocity changed from the middle level to the small level in Fig. 13(c). The NMSE records in Fig. 13(b) and (c) are 0.0029 and 0.0026, respectively. It is obvious that the single-stage boost inverter with the proposed FNN control system can work well for real household appliances.

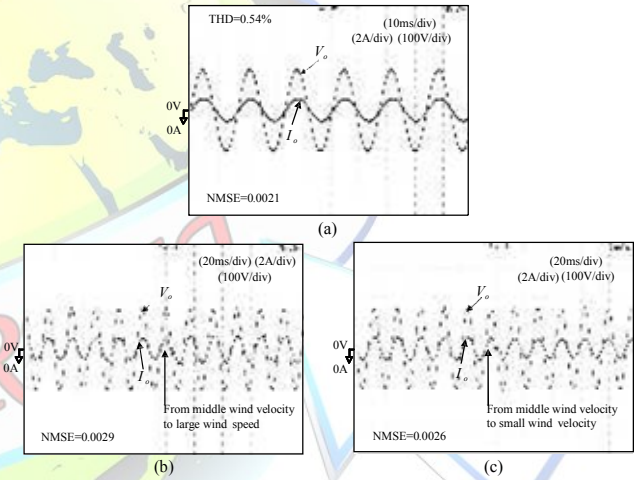

Fig. 13. Experimental results of boost inverter with FNN control for electric fan applications: (a) Middle wind velocity; (b) Wind velocity changes from middle level to large level; (c) Wind velocity changes from middle level to small level.

ISSN 2394-3777 (Print)
ISSN 2394-3785 (Online)
Available online at www.ijartet.com

International Journal of Advanced Research Trends in Engineering and Technology (IJARTET)
Vol. 2, Issue 9, September 2015

Figure 14 summarizes the conversion efficiency of the single-stage boost inverter under different powers. On the experimental system, the converter efficiency is evaluated via Power Analyzer PA4400A equipment, manufactured by the AVPower Company. The bandwidth of the PA4400A is dc to 500kHz, and the accuracy of the measured power is within ±0.1%. From this experimental result, the maximum conversion efficiency is about 86.4% at the output power of 364W, and the conversion efficiency at the maximum output power 1kW is 82%. As a result, the maximum conversion efficiency 86.4% of the single-stage boost inverter should be equivalently both the power conversion efficiencies of a two-stage framework including a dc-dc boost converter and a dc-ac inverter over 93%. Even for the conversion efficiency 82% at the maximum output power 1kW, both the power conversion efficiencies of a two-stage framework should be over 91%. Besides, there are severe voltage/current ripples with twice of output ac frequency in

ISSN 2394-3777 (Print)
ISSN 2394-3785 (Online)
Available online at www.ijartet.com

International Journal of Advanced Research Trends in Engineering and Technology (IJARTET)
Vol. 2, Issue 9, September 2015

the high-voltage bus as for a two-stage framework [7]. One can conclude that the objective of high-efficiency power conversion can be achieved by the adopted single-stage boost converter in this study.

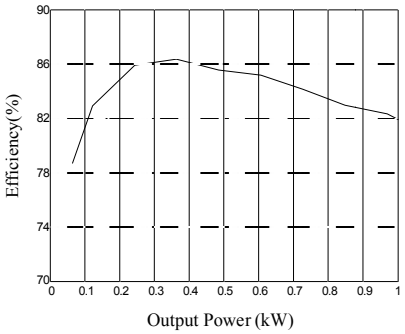

Fig. 14. Conversion efficiency of single-stage boost inverter under different powers.

V. CONCLUSION

This study has successfully implemented a double-loop proportional-integral (PI) control framework, an adaptive control scheme and a fuzzy neural network (FNN) control system with varied learning rates for a single-stage boost inverter to demonstrate their individual control diversities. The quantitative and qualitative performance comparisons of the double-loop PI control framework, the adaptive control scheme, and the FNN control system are given in Table II. The PI control framework belongs to an event-based linear controller. There are larger total harmonic distortion (THD) and normalized-mean-square-error (NMSE) values under the occurrence of power variations; therefore, the control gains should be retuned due to different operational conditions. Moreover, the proposed adaptive control scheme not only has good tracking response, but also makes this system more robust under different operational conditions. However, this scheme requires detailed system information. In addition, the FNN control system with varied learning rates is presented to solve this problem. It can be designed successfully without complex mathematical dynamic model, and possesses smaller THD and NMSE values. As can be seen from Table II, the proposed FNN control system has 14.4% THD and 29.3% NMSE improvements at the condition of 1kW output power than the conventional double-loop PI control framework. Due to the on-line learning ability of the FNN, the proposed FNN control system at the condition of nonlinear load has significant improvements of 45.2% THD and 37.1% NMSE compared to the conventional double-loop PI control framework. Although the adopted double-loop PI control framework is a model-free control design similar to the proposed FNN control system, the PI gains usually need manual retuning before being transferred to the process under different operational conditions.

In this study, the proposed adaptive control scheme belongs to a model-based control framework, and the corresponding control performance is easily affected by system distortion and parameter changes. Even though the introduction of identification of possible changes in the load parameters caused by the circumstances into the proposed adaptive control scheme may improve the control performance, it will result in a more complicated control framework, and the system stability is a latent problem to be challenged. From these performance comparisons, the FNN control system with varied learning rates is more suitable to control the single-stage boost inverter than the PI control and adaptive control schemes, even though it requires a high computation amount.

The major contributions of this application-oriented study are summarized as follows. (i) The successful derivation of the dynamic model of a single-stage boost inverter to design a model-based adaptive control scheme.
(ii) The successful development of a model-free FNN control system with varied learning rates for a single-stage boost inverter to relax the requirement of detailed system information in the adaptive control scheme. (iii) The successful comparisons of individual control performances to provide designers with preliminary guideline for manipulating this single-stage boost inverter efficiently. Although the developed boost inverter plus the voltage tracking control design belongs to a stand-alone application, it can further add a grid-connected inductor and modify the voltage-type boost inverter control into a current-type one to form a grid-connected power-supply framework in the future.

TABLE II.
QUANTITATIVE AND QUALITATIVE PERFORMANCE COMPARISONS

Control System			PI control	Adaptive control	FNN control
Improvement Rate	THD	Output power 1kW	Baseline	8%	14.4 %
		Nonlinear load	Baseline	36.6%	45.2 %
	NMSE	Output power 1kW	Baseline	20.3%	29.3 %
		Nonlinear load	Baseline	25.2%	37.1 %
Dependence on system parameter			Low	High	None
Learning ability			None	None	On-line learning
Computation burden			Low	Low	High

ISSN 2394-3777 (Print)
ISSN 2394-3785 (Online)
Available online at www.ijartet.com

International Journal of Advanced Research Trends in Engineering and Technology (IJARTET)
Vol. 2, Issue 9, September 2015

REFERENCES

[1] G. D. Wang, R. J. Wai, and Y. Liao, "Design of backstepping power control for grid-side converter of voltage source converter-based high voltage dc wind power generation system," *IET Renew. Power Gener.*, vol. 7, no. 2, pp. 118-133, 2013.

[2] J. W. Chen, J. Chen, and C. Y. Gong, "On optimizing the transient load of variable-speed wind energy conversion system during the MPP tracking process," *IEEE Trans. Ind. Electron.*, vol. 61, no. 9, pp. 4698-4706, 2014.

[3] R. J. Wai, W. H. Wang, and C. Y. Lin, "High-performance stand-alone photovoltaic generation system," *IEEE Trans. Ind. Electron.*, vol. 55, no. 1, pp. 240-250, 2008.

[4] G. Buticchi, D. Barater, E. Lorenzani, C. Concari, and G. Franceschini, "A nine-level grid-connected converter topology for single-phase transformerless PV systems," *IEEE Trans. Ind. Electron.*, vol. 61, no. 8, pp. 3951-3960, 2014.

[5] R. J. Wai, S. J. Jhung, J. J. Liaw, and Y. R. Chang, "Intelligent optimal energy management system for hybrid power sources including fuel cell and battery," *IEEE Trans. Power Electron.*, vol. 28, no. 7, pp. 3231-3244, 2013.

[6] X. W. Pan and A. K. Rathore, "Novel bidirectional snubberless naturally commutated soft-switching current-fed full-bridge isolated dc/dc converter for fuel cell vehicles," *IEEE Trans. Ind. Electron.*, vol. 61, no. 5, pp. 2307-2315, 2014.

[7] R. J. Wai and C. Y. Lin, "Dual active low-frequency ripple control for clean-energy power-conditioning mechanism," *IEEE Trans. Ind. Electron.*, vol. 58, no. 11, pp. 5172-5185, 2011.

[8] R. O. Cáceres and I. Barbi, "A boost DC-AC converter: analysis, design, and experimentation," *IEEE Trans. Power Electron.*, vol. 14, no. 1, pp. 134-141, 1999.

[9] G. Escobar, A. A. Valdéz, J. Leyva-Ramos, and P. R. Martínez, "A controller for a boost converter with harmonic reduction," *IEEE Trans. Control Syst. Technol.*, vol. 12, no. 5, pp. 717-726, 2004.

[10] T. T. Song and H. S. Chung, "Boundary control of boost converters using state-energy plane," *IEEE Trans. Power Electron.*, vol. 23, no. 2, pp. 551-563, 2008.

[11] R. J. Wai and L. C. Shih, "Design of voltage tracking control for DC-DC boost converter via total sliding-mode technique," *IEEE Trans. Ind. Electron.*, vol. 58, no. 6, pp. 2502-2511, 2011.

[12] R. J. Wai and L. C. Shih, "Adaptive fuzzy-neural-network design for voltage tracking control of a dc-dc boost converter," *IEEE Trans. Power Electron.*, vol. 27, no. 4, pp. 2104-2115, 2012.

[13] Y. M. Roshan and M. Moallem, "Control of nonminimum phase load current in a boost converter using output redefinition," *IEEE Trans. Power Electron.*, vol. 29, no. 9, pp. 5054-5062, 2014.

[14] D. Cortes, Jq. Alvarez, J. Alvarez, and A. Fradkov, "Tracking control of the boost converter," *IEE Proc. Contr. Theory Appl.*, vol. 151, no. 2, pp. 218-224, 2004.

[15] P. Sanchis, A. Ursœa, E. Gubía, and L. Marroyo, "Boost DC-AC inverter: a new control strategy," *IEEE Trans. Power Electron.*, vol. 20, no. 2, pp. 343-353, 2005.

[16] M. Jang and V. G. Agelidis, "A minimum power-processing-stage fuel-cell energy system based on a boost-inverter with a bidirectional backup battery storage," *IEEE Trans. Power Electron.*, vol. 26, no. 5, pp. 1568-1577, 2011.

[17] M. Jang, M. Ciobotaru, and V. G. Agelidis, "A single-phase grid-connected fuel cell system based on a boost-inverter," *IEEE Trans. Power Electron.*, vol. 28, no. 1, pp. 279-288, 2013.

[18] L. S. Garcia, G. M. Buiatti, L. C. de Freitas, E. A. A. Coelho, V. J. Farias, and L. C. G. de Freitas, "Dual transformerless single-stage current source inverter with energy management control strategy," *IEEE Trans. Power Electron.*, vol. 28, no. 10, pp. 4644-4656, 2013.

[19] S. Danyali, S. H. Hosseini, and G. B. Gharehpetian, "New extendable single-stage multi-input DC–DC/AC boost converter," *IEEE Trans. Power Electron.*, vol. 29, no. 2, pp. 775-788, 2014.

[20] K. J. Astrom and T. Hagglund, *PID Controller: Theory, Design and Tuning*. NC: ISA, 1995.

[21] K. J. Astrom and B. Wittenmark, *Adaptive Control*. NY: Addison Wesley, 1995.

[22] L. X. Wang, *A Course in Fuzzy Systems and Control*. NJ: Prentice-Hall, 1997.

[23] O. Omidvar and D. L. Elliott, *Neural Systems for Control*. Academic Press, 1997.

[24] C. T. Lin and C. S. George Lee, *Neural Fuzzy Systems*. NJ: Prentice-Hall, 1996.

[25] R. J. Wai and C. M. Liu, "Design of dynamic petri recurrent fuzzy neural network and its application to path-tracking control of nonholonomic mobile robot," *IEEE Trans. Ind. Electron.*, vol. 56, no. 7, pp. 2667-2683, 2009.

[26] N. Mohan, T. M. Undeland, and W. P. Robbins, *Power Electronics: Converters, Applications, and Design*. NY: Johh Wiely & Sons Inc., 1995.